

# Deformable model based computation of ejection fraction of right ventricle from cine MRI.

Soumya Ghose

**Abstract**—The ejection fraction of the right ventricle is an important indicator for various diseases like dysplasia, cardiomyopathy and pulmonary artery stenosis. Ejection fraction of the right ventricle is computed from cardiac MRI that generates a huge volume of images. In clinical practice, manual tracing of the contour of the right ventricle in MRI images is done in the systolic and diastolic stages of the heart. Difference in the volume of ventricular blood computed from manual tracing of the right ventricle in systolic and diastolic stages is used to determine the ejection fraction. However, this approach has two problems. All the images generated in cardiac MRI are not manually post-processed and the contours are manually traced. Therefore, computation of the volume of blood suffers from personal bias, and inter-observer variations. The objective of this thesis is to segment the right ventricle using active contour model. Additionally, automatic computation of the volume and ejection fraction of the right ventricle from segmented right ventricle eliminates personal bias and inter-observer variations. Segmented contour points of the right ventricle are used to generate a 3D mesh using Delaunay's triangulation.

## I. INTRODUCTION

The heart is a vital organ of the human circulatory system. Proper functioning of the heart is essential to prevent cardio vascular diseases. Lack of cardio vascular exercise, sedentary and stressed lifestyle, unhealthy diet, diabetes and genetic factors, all contribute to the development of cardio vascular disorders. According to the latest statistics [1] released by the European Heart Network, cardio vascular disease is the primary cause of all deaths in the European Union. Regular examination and monitoring of individuals in the high risk group is essential in keeping down the rate of cardio vascular diseases in the society. Traditionally, blood pressure monitoring, blood test for detecting cholesterol and ECG were considered as the only options for monitoring cardio vascular health of an individual. However, with the advancements in medical science and development of new technologies, the examination of an individual with respect to cardio vascular diseases has seen some major changes. In recent years, different imaging modalities like echocardiography, computer tomography, MUGA scan, scintigraphy and magnetic resonance imaging are all used for studying the heart. Magnetic Resonance Imaging (MRI) with high spatial and temporal resolutions is well suited for the study of the heart. MRI examination of a single patient generates a significant volume of data. Analysis of these data by

radiologists or the doctors is time consuming and suffers from personal bias and inter personal assessment differences. Therefore, with the increase in number of cardio vascular disease patients in the society, application of computers in image processing and analysis could provide a solution.

The last few decades have seen a rapid advancement in the development of robust techniques in the domain of image processing and pattern recognition. Many of these techniques have been successfully employed to solve problems in the domain of medical science. Fig. 1 shows different stages in a typical computer vision system. The system initialises with the acquisition of the image. Different image processing techniques are employed to remove noise or artefacts to make the image suitable for information extraction. The next stage of the system would be image segmentation. The goal of image segmentation is partitioning of the image into non overlapping regions with homogeneous characteristics like grey scale value or texture.



Fig. 1. A computer vision system

Image segmentation is followed by feature extraction. Feature extraction helps in reduction of volume of data for an image without compromising information. It is a procedure of extraction of meaningful data that is necessary for pattern recognition. The objective of pattern recognition is to classify features into groups with homogeneous characteristics. Pattern recognition is a necessary step in decision making, for example, determining diseased or normal state for a patient. Hence, it is evident that medical image segmentation plays a crucial role in delineation of regions of interest under study. Medical image segmentation is essential in almost any medical imaging applications. It is an essential step towards automated disease state detection in diagnostic imaging.

An image in computer vision system could be defined as a two dimensional or three dimensional matrix of pixels, where each pixel corresponds to a definite intensity value. In medical imaging, these intensities could be radiation absorbed during x- ray, or acoustic pressure in ultrasonography, or radio frequency signals in MRI. Image segmentation is a procedure in which an image is divided into regions of some homogeneous characteristics like grey scale value, colour or texture. Thus, if the domain of the image is considered as  $\omega$ , then the goal of image segmentation is to find  $S_k$  [2] such that

$$\omega = \bigcup_{k=1}^n S_k \quad (1)$$

and  $S_i \cap S_j = \phi$  for  $i \neq j$ .

Medical image segmentation can be broadly categorised into two domains, region based segmentation and contour based segmentation. Region based segmentation using active contour models is common in medical imaging. Restriction of maintaining a smooth contour makes active contour models more robust against noise [2]. Active contour models could be prevented from getting trapped into false edges by incorporating shape prior information. With low noise sensitivity and low time complexity, active contour models are well suited for segmentation of dynamic structures like the heart.

## II. STATE OF THE ART : ACTIVE CONTOUR MODELS

### A. Active Contour Model : Internal Energy

Active contour model or snake was developed by three researchers Kass, Witkin and Terzopoulos [3]. Active contour models can be considered as an energy optimization problem that tries to minimize the sum of internal and external energies of a contour. Classically, minimization of internal energy ensures preservation of smooth contour and minimization of external energy ensures improved localisation and fitting of the active contour on real edges. Kass et al. [3] proposed spline as active contour. They proposed internal energy of an active contour model as the  $1^{st}$ -order and the  $2^{nd}$ -order derivatives of the spline, with a weight associated with each component as shown in (2)

$$\begin{aligned} \text{Internal Energy} = & \frac{1}{2} \int_0^1 \alpha \left( \left| \frac{dX}{ds} \right|^2 + \left| \frac{dY}{ds} \right|^2 \right) \\ & + \beta \left( \left| \frac{d^2X}{ds^2} \right| + \left| \frac{d^2Y}{ds^2} \right| \right) ds. \quad (2) \end{aligned}$$

In (2),  $s$  denotes the spline and  $(X, Y)$  is a location on the spline. The  $1^{st}$ -order and the  $2^{nd}$ -order derivatives in (2) ensure smoothness. The  $1^{st}$ -order component is known as the stretching energy (tension) and it prevents the snake from being stretched. The  $2^{nd}$ -order component is called the bending energy (rigidity) and prevents bending of the snake reducing sharp edges. Presence of  $1^{st}$ -order and the  $2^{nd}$ -order derivative components in internal energy ensures second order parametric continuity. Zero order parametric continuity ensures that the curve passes through the boundary points, first order parametric continuity ensures that zero order is maintained and the first derivative of the curve exists at the boundary points. Second order parametric continuity means that first order parametric continuity is maintained and the second derivative exists in the boundary points. It is evident from the discussion that higher degree of parametric continuity ensures greater degree of smoothness [4]. Hence, presence of second order parametric continuity ensures a smooth contour in the classical active contour model framework.

### B. Active Contour Model : External Energy

Classically, external energy term ensures fitting of the active contour to a desired location, the edge. The external energy of active contour model according to Kass et al. is defined as the squared image gradient magnitude in (3).

$$f(x, y) = |\nabla I(x, y)|^2. \quad (3)$$

Presence of gradient near the edges ensures that the active contour follows the direction of the gradient in progressive deformation and stops at the edge when initialised closed to the contour.

### C. Active Contour Model : Energy Minimization

The total energy of the snake is given by (4).

$$\begin{aligned} E(X, Y) = & \frac{1}{2} \int_0^1 \alpha \left( \left| \frac{dX}{ds} \right|^2 + \left| \frac{dY}{ds} \right|^2 \right) \\ & + \beta \left( \left| \frac{d^2X}{ds^2} \right| + \left| \frac{d^2Y}{ds^2} \right| \right) ds \\ & - \int_0^1 f[X(s), Y(s)] ds. \quad (4) \end{aligned}$$

The negative sign in front of the external energy implies maximising the sum of image gradient magnitude over the entire contour will minimize the total external energy. To minimize the snake total energy, the following conditions must be satisfied,

$$\begin{aligned} E'(X, Y) &= 0 \\ E''(X, Y) &> 0. \end{aligned}$$

The problem that lies in such a minimization is that  $E(X, Y)$  is a function of the snake location  $(X, Y)$  which itself is a function of  $s$ , i.e.  $E(\cdot)$  is a function of a function. Therefore, variational calculus is required to perform the energy minimization. Using variational calculus and taking first derivative of (4) with respect to  $X$  and  $Y$  we have the Euler equations. Equating the Euler equation equal to zero as in (5) and (6) we have,

$$\frac{\partial E}{\partial X} = -\alpha \frac{d^2X}{ds^2} + \beta \frac{d^4X}{ds^4} - \frac{\partial f}{\partial x} = 0 \quad (5)$$

$$\frac{\partial E}{\partial Y} = -\alpha \frac{d^2Y}{ds^2} + \beta \frac{d^4Y}{ds^4} - \frac{\partial f}{\partial y} = 0. \quad (6)$$

In (5) and (6),  $f(\cdot)$  is the potential surface or external force. The Euler equations are solved by gradient descent method. According to gradient descent algorithm, we try to reach the minimum energy where the velocity of each point on the contour will be zero as shown in (7) and (8)

$$\frac{\partial X}{\partial \tau} = \alpha \frac{d^2 X}{ds^2} - \beta \frac{d^4 X}{ds^4} + \frac{\partial f}{\partial x} = 0 \quad (7)$$

$$\frac{\partial Y}{\partial \tau} = \alpha \frac{d^2 Y}{ds^2} - \beta \frac{d^4 Y}{ds^4} + \frac{\partial f}{\partial y} = 0. \quad (8)$$

This can be interpreted as a force that drives the snake towards minimum energy. The resultant force is composed of two components; the internal force that prevents bending and stretching and the external force that drives the snake towards image edge [5].

#### D. Different External Forces

The classical approach of Kass et al. uses squared image gradient magnitude as the basis of snake external force. However, external energy computed from image gradient is often susceptible to noise and detects false edges. Moreover, initialization of a snake in a homogeneous region fails to converge. The image gradient is zero in homogeneous regions, therefore no edge force would act on the snake to push the snake contour towards the desired edges. Hence, active contour model based on gradient magnitude as external energy is initialization dependent and has limited capture range [5]. Likewise, different energy potential as external force has been developed over the years.

Distance potential force proposed by Cohen and Cohen [6] is a solution to the limitation of gradient potential force in case of binary images. Here, the distance surface acts as a source of snake external force.

A balloon force tries either to inflate or deflate a closed contour [7]. It exerts a force that is normal to the active contour (outward or inward).

Gradient vector flow (GVF) was proposed by Xu and Prince [8]. In GVF, an external force field  $(u(x, y), v(x, y))$  is constructed by diffusing edge force  $(f_x, f_y)$  away from the edges to homogeneous regions at the same time keeping the constructed field as close as possible to the edge force near the edges. The goal is achieved by minimising the following energy function in (9).

$$E_{GVF}(u, v) = \frac{1}{2} \int \int \mu (u_x^2 + u_y^2 + v_x^2 + v_y^2) + (f_x^2 + f_y^2) ((u - f_x)^2 + (v - f_y)^2) dx dy \quad (9)$$

where,  $\mu$  is the non-negative parameter expressing the degree of smoothness of the field  $(u, v)$ .

In (9), the first integrand keeps the field smooth. It is similar to the classical Laplace's equation. The second integrand forces the vector field to resemble the initial edge force near the edge (i.e. where the edge force is high). Solving (9) the Euler equations obtained are shown in (10) and (11).

$$\mu \nabla^2 u - (f_x^2 + f_y^2)(u - f_x) = 0 \quad (10)$$

$$\mu \nabla^2 v - (f_x^2 + f_y^2)(v - f_y) = 0. \quad (11)$$

Solving the above equations for  $(u, v)$  results in GVF that acts as an external force. Snake evolution becomes as in (12) and (13).

$$\frac{\partial X}{\partial \tau} = \alpha \frac{\partial^2 X}{\partial s^2} - \beta \frac{\partial^4 X}{\partial s^4} + u(X, Y) \quad (12)$$

$$\frac{\partial Y}{\partial \tau} = \alpha \frac{\partial^2 Y}{\partial s^2} - \beta \frac{\partial^4 Y}{\partial s^4} + v(X, Y). \quad (13)$$

Some preliminary experiments were performed for justifying the selection of gradient vector flow over other external forces for the active contour model. The results are shown in fig. 2.

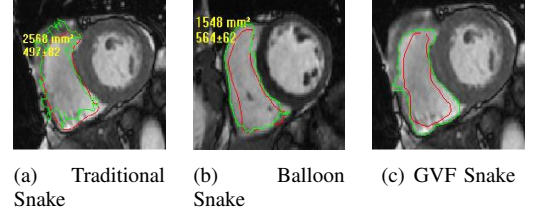


Fig. 2. Performance Comparison of Traditional, Balloon and GVF Snake.

It was assumed that the concave shape of the right ventricle in the testing slice does not allow the traditional and the balloon snakes to converge. All the external forces discussed above do not allow concavity of the snake other than gradient vector flow.

### III. METHODOLOGY

Literature review of segmentation of heart from MRI data shows that very little work has been done in segmentation of the right ventricle and there are different reasons for this. In most cases, cardiomyopathy can be determined from the ejection fraction of the left ventricle. Thus, more research has been dedicated in the segmentation of the left ventricle. Difficulties faced in modelling the right ventricle is the second reason why very little research has been contributed to the segmentation of the right ventricle. The left ventricle with a well defined hemispherical shape is easy to model and segment. The shape of the right ventricle is asymmetric, and changes abruptly between the basal and the apical region. Also, the translational and long axis movements of the right ventricle create different shapes for the same slice that is not easily definable geometrically. However, accurate computation of the right ventricular ejection fraction is necessary in determining heart diseases associated with the right ventricular function. The method proposed uses active contour model for segmentation of the right ventricle. Gradient vector flow as an external force is used for driving the active contour or the snake to the real edge. Summarizing the method developed in terms of algorithm for computing ejection fraction and generating a 3D model we have the following,

- 1) Normalization and signal enhancement.
- 2) Binary thresholding of the image.
- 3) Apply morphological operators opening and closing.
- 4) Compute gradient magnitude of the image.
- 5) Compute gradient vector flow from the gradient magnitude.

- 6) Initialize the snake at the basal region of the right ventricle.
- 7) Iteratively deform and interpolate snake under the influence of the internal and external forces.
- 8) Compute termination threshold after each iteration.
- 9) Terminate snake on reaching edge or meeting the termination threshold.
- 10) On termination, use the snake to initialize next slice temporally and spatially.
- 11) Iterate until all the slices have been processed in temporal and spatial domain.
- 12) Compute ejection fraction and generate mesh.

Stepwise explanation of the different stages of the algorithm is as follows,

#### A. Image Normalization

The image is normalized using (14)

$$E = 1 - I/M \quad (14)$$

In (14),  $I$  is the intensity at any pixel,  $M$  is the maximum intensity of the image. Xu and Prince [8] mentioned that (14) normalizes the intensity values between zero to one maintaining high values near the edges.

#### B. Image Preprocessing

Adaptive binary thresholding followed by opening and closing morphological operators ensure a smooth contour for the right ventricle in the image preprocessing step. The average grey scale value of the initialized snake contour points is used as the threshold value. It is assumed that the user initializes the snake inside the right ventricle making the average of the contour points an appropriate value for thresholding the image. The selection of the threshold value in this manner ensures adaptive but correct representation of the right ventricle threshold value, providing flexibility and robustness to the algorithm. Opening and closing morphological operations ensure smooth contour. Opening operation breaks narrow isthmuses and eliminates thin protrusions in the contour while closing operation fuses narrow breaks and long thin gulfs, eliminates small holes and fills gap in the contour [9].

#### C. Gradient Vector Flow

Gradient Vector Flow (GVF) of the image acts as the external force for driving the active contour towards the edge. Gradient of the processed image is computed using (15) [8].

$$\nabla f = \begin{bmatrix} G_x \\ G_y \end{bmatrix} = \begin{bmatrix} \frac{\partial f}{\partial x} \\ \frac{\partial f}{\partial y} \end{bmatrix} \quad (15)$$

The magnitude of the gradient vector of the image is computed using (16).

$$\nabla f = \text{mag}(\nabla f) = [G_x^2 + G_y^2]^{\frac{1}{2}} \quad (16)$$

Gradient vector flow of the gradient magnitude of the processed image is computed using (17). Xu and Prince

proposed that gradient vector flow as external energy ensures that the gradient vector field is maintained near the edges at the same time maintaining a smooth diffusion of the edges.

$$E_{GVF}(u, v) = \frac{1}{2} \int \int \mu(u_x^2 + u_y^2 + v_x^2 + v_y^2) + (f_x^2 + f_y^2)((u - f_x)^2 + (v - f_y)^2) dx dy \quad (17)$$

#### D. Active Contour Initialization

The snake is initialized inside the right ventricle. The control points of the snake are used to build a double circular linked list. Creation of such a list allows flexibility in addition, modification, deletion and display of control points of the snake during execution time. Making the list circular helps in maintaining a closed contour and making the list doubly linked allows easy modification and deletion of any node.

#### E. Active Contour Interpolation

The Euclidean distance between the control points are of variable lengths. Snake interpolation normalizes the length between the control points by maintaining maximum and minimum distance ensuring better contour fitting and smoothness.

#### F. Active Contour Deformation

Depending on the energy minimization criteria of Kass et al. [3] snake deform or evolution equation for the spline point  $(\mathbf{x}, \mathbf{y})$  is given in (18) and (19) respectively.

$$\begin{aligned} \frac{\mathbf{x}^{\tau+1} - \mathbf{x}^{\tau}}{\zeta} &= -A\mathbf{x}^{\tau+1} + f_x^{\tau} \\ \mathbf{x}^{\tau+1}(I_n + \zeta A) &= \mathbf{x}^{\tau} + \zeta f_x^{\tau} \\ \mathbf{x}^{\tau+1} &= (I_n + \zeta A)^{-1}(\mathbf{x}^{\tau} + \zeta f_x^{\tau}) \end{aligned} \quad (18)$$

and similarly,

$$\begin{aligned} \frac{\mathbf{y}^{\tau+1} - \mathbf{y}^{\tau}}{\zeta} &= -A\mathbf{y}^{\tau+1} + f_y^{\tau} \\ \mathbf{y}^{\tau+1} &= (I_n + \zeta A)^{-1}(\mathbf{y}^{\tau} + \zeta f_y^{\tau}) \end{aligned} \quad (19)$$

In (18) and (19)  $A$  is the parametric matrix maintaining the spline parametric continuity and  $f_x$  and  $f_y$  are the gradient vector flow force in  $X$  and  $Y$  directions respectively. Parametric matrix  $A$  ensures smoothness of the contour.  $f_x$  and  $f_y$  are the external forces that deform the snake towards the contour. Snake is deformed and interpolated iteratively to converge on the contour.

#### G. Active Contour Termination Condition

Normalized snake length proposed by Wong et al. [10] is taken as the termination criteria for snake deformation and interpolation. Normalized length  $\varepsilon$  is computed using (20).

$$\varepsilon = \left| \frac{\frac{1}{p} \sum_{i=m-p+1}^m l^i - \frac{1}{p} \sum_{k=m-2p+1}^{m-p} l^k}{\frac{1}{p} \sum_{i=m-p+1}^m l^i} \right|$$

$$= \left| \frac{\sum_{i=m-p+1}^m l^i - \sum_{k=m-2p+1}^{m-p} l^k}{\sum_{i=m-p+1}^m l^i} \right| \quad (20)$$

In (20)  $p$  denotes the number of points  $i$  and  $k$  denotes different iteration steps for the snake. After every iteration the rate of change of normalized length is obtained. If the rate falls below a certain threshold the snake terminates. The snake terminates either on reaching the contour or on meeting the termination criteria.

#### H. Active Contour Fitting

Gradient vector flow as external force was able to push the snake very close to the contour. However, it was not possible to have a perfect fit for the snake on the real contour of the right ventricle. A new heuristic curve fitting algorithm is developed ensure the snake fit on the contour. The algorithm can be summarized as,

- 1) Take a small window around each control point.
- 2) Find the maximum gradient magnitude in the window.
- 3) Compare the magnitude value with the magnitude value of the control point.
- 4) Do nothing if the magnitude of the control point is higher.
- 5) Move the control point to the position of maximum magnitude if the magnitude of the control point is less than maximum magnitude.

The snake fitting algorithm pushes the snake control points to the contour of the right ventricle. The method exploits the fact that there is a presence of high magnitude of gradient value in the real contour. The method works well due to the fact that the final position of the snake obtained without the heuristic is visually very close to the image contour.

#### I. Active Contour Propagation

The snake obtained in the previous slice is used to initialize the next slice in both spatial and temporal resolution. The snake propagates in spatial and temporal domain segmenting the contour of the right ventricle.

#### J. Ejection Fraction Computation

On segmentation of the right ventricle in all the slices in spatial and temporal resolution, area of the snake in each slice is computed using (21).

$$A = \frac{1}{2} \sum_{i=0}^{n-1} (x_i y_{i+1} - y_i x_{i+1}) \quad (21)$$

In (21)  $i$  denotes the number of points in the snake contour. Volume for the right ventricle is computed for every temporal

resolution. Contiguous short axis slice models using (22) are used for determining the volume of the right ventricle.

$$V = T \sum_{i=1}^n A_i \quad (22)$$

In (22)  $V$  denotes the right ventricular volume,  $T$  denotes the slice thickness and  $A_i$  denotes the area of the right ventricular cavity for the  $i^{th}$  slice.

The equation used for computation of ejection fraction is given as in (23).

$$EF = (DV - SV)/DV \times 100 \quad (23)$$

In (23)  $EF$  denotes ejection fraction,  $DV$  denotes diastolic volume and  $SV$  denotes systolic volume.

#### K. Mesh Creation

Delaunay's triangulation is used to produce three dimensional meshes in spatial domain at each temporal resolution using the extracted and generated contour coordinates. Delaunay's triangulation ensures that for a set of points  $P$ , triangulation of these  $P$  points will be done such that no element of set  $P$  lies in the circumcircle of any triangle.

## IV. RESULTS AND DISCUSSIONS

The results of the proposed and implemented algorithms are summarized below. Fig. 3 shows image normalization and adaptive binary thresholding for an image slice.

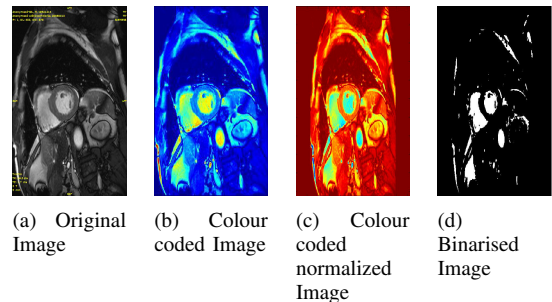


Fig. 3. Normalized and binarised images.

The region of interest in the figures shown will be the right ventricle. Fig. 4 shows how the problem of rough contour in binarised image was solved using morphological operations.

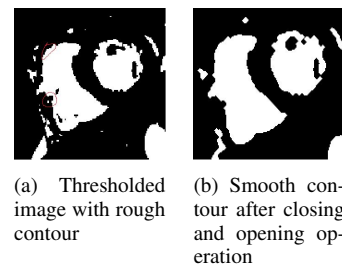


Fig. 4. Application of Morphological Operators.

Fig. 5(a) shows the gradient of the processed image. Fig. 5(b) shows GVF force in horizontal direction and fig. 5(c) shows GVF force in vertical direction. Fig. 5(d) shows the directional map of GVF force, fig. 5(e) shows the zoomed view of the heart in directional map and fig. 5(f) shows the zoomed view of an edge in GVF map. The red mask in fig. 5(e) shows the region that was zoomed.

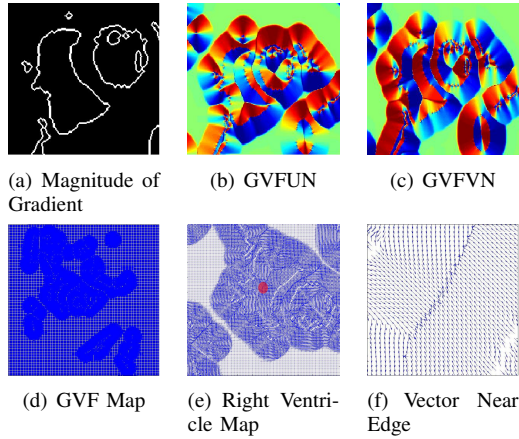


Fig. 5. Gradient Vector Flow Map.

Fig. 6(a) shows the initialization of the snake marked in red, fig. 6(b) shows the final fit for the snake in green, fig. 6(c) shows the problem in snake fitting and fig. 6(d) shows snake fit obtained after the application of the heuristic fitting algorithm.

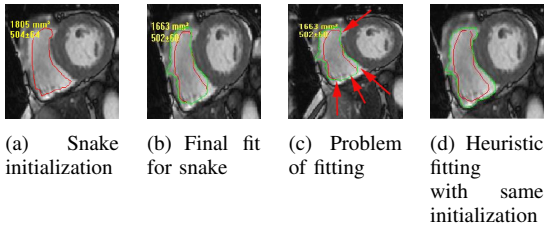


Fig. 6. Snake fitting with and without snake fitting algorithm

Fig. 7 shows the propagation of active contour. Fig. 7(b) shows spatial propagation and fig. 7(c) shows the propagation of the same slice in temporal resolution.

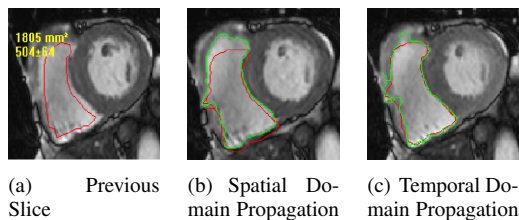


Fig. 7. Snake Propagation.

The cloud of points generated during right ventricular segmentation is used to form a 3D mesh using Delaunay's triangulation. 3D mesh is created at each temporal resolution.

Fig. 8(a) shows the structure of right ventricle in diastolic stage and fig. 8(b) shows the right ventricular structure in systolic stage. The difference in volume is evident from the mesh.

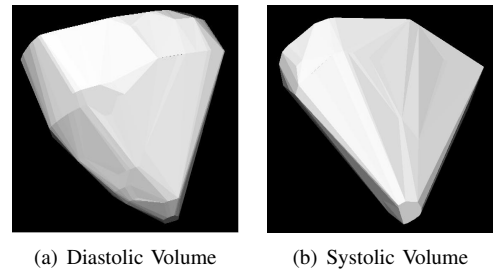


Fig. 8. Mesh Generation.

Comparing the active contour generated in the basal region as shown in fig. 9(a) with manual tracing of the same slice as shown in fig. 9(b) we find a close approximation. However, the results are not so good in the middle slices as shown in fig. 9(c).

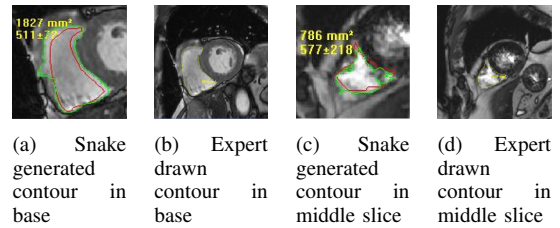


Fig. 9. Contour detection

The ejection fraction graph is generated on completion of processing of all the images in spatial and temporal resolution. As discussed, false detection in the middle and the apical region of the right ventricle generates erroneous volume. The green line in graph 10 shows the detected volume and the blue line shows the graph that should have been obtained. The problem region is encircled in red. This results in under estimation of the ejection fraction as given in table I.

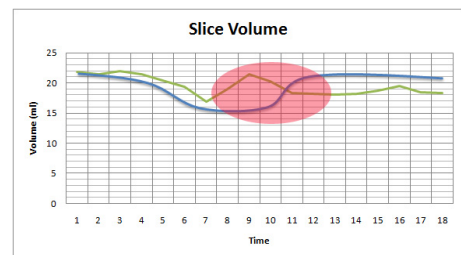


Fig. 10. Right ventricular volume in different cardiac cycle

## V. CONCLUSIONS AND FUTURE WORK

### A. Conclusions

The segmentation of the right ventricle using active contour model was proposed. Adaptive binary thresholding and

Ejection Fraction/Detection	Manual tracing	Active contour model
Ejection Fraction	34	23

TABLE I  
EJECTION FRACTION COMPUTATION

opening and closing morphological operators produced a smooth contour. The capture range of the active contour was improved using a gradient vector flow as external energy for the active contour. Gradient vector flow ensured pushing the contour into regions of concavity in the right ventricle. A close fit of the active contour to the real contour was achieved using the gradient vector flow map. However, the final fitting of the active contour was achieved using a heuristic snake fitting algorithm developed for the purpose. Normalized length of the active contour was used as the termination criteria. The snake obtained in one slice was used to initialize the next slice in spatial and temporal resolution. The active contour propagated in temporal and spatial resolution generating segmented right ventricle. Segmented right ventricle in spatial resolution was used to generate a three dimensional model for every temporal resolution. Delaunay's triangulation was used to generate a three dimensional mesh from the cloud of points generated during segmentation in the spatial resolution. Volume versus time curve of the right ventricle was generated. The diastolic and the systolic volume of the curve was computed from maxima and minima of the curve. Ejection fraction of the right ventricle was obtained using the systolic and diastolic volumes.

Six datasets with variable environmental noise and artefacts were used for validating the segmentation results. Initial results show a good approximation of the contour when compared to manual segmentation in the basal region of right ventricle. However, better results could be achieved in the apical and the middle slices of the right ventricle. Propagation of the active contour model proved to be more difficult in the middle and the apical region of right ventricle.

### B. Future Works

Smoother and better detection of the right ventricular contour is specially important in the base as it contains maximum volume of blood. Active contour models often produced rough edges and protrusions that needed to be smoothed. *Moving average* of the detected contour could be used to generate a smooth contour. *Cumulative average* of the previously detected contours could also be used for obtaining a smooth contour. *Shape prior* of the right ventricle computed from the expert drawn contour for the first slice could be used for smoothing the detected contour. *Cubic bezier* could be used to approximate the detected contour. This would help in reducing computational complexity and obtaining a smoothed contour. Propagation of snake from one slice to another in spatial resolution is affected by the abrupt change of the right ventricle producing erroneous detection. Probably, using shape prior model will facilitate a better detection of the contour specially in the middle and the

apical regions. *Shape morphing* from one slice to another in spatial resolution would generate the intermediate contours between two slices. This could also be instrumental in obtaining a better three dimensional mesh. Shape morphing would also allow the doctors to *study the flow of blood* and detect abnormalities. Two dimensional MRI images of every slice could be projected in the three dimensional mesh. This will allow the doctors to check for abnormalities in a particular slice. The ejection fraction computed could be used as clinical routine in monitoring patient health. Finally, a *pattern recognition* method could be developed that incorporates different features like height, weight, ejection fraction, exercise frequency, blood pressure, cholesterol etc. for automatic detection of a pathological state.

## VI. ACKNOWLEDGMENTS

I would like to thank all the teachers of the collaborating universities of Master's VIBOT without whose lectures and guidance the project would not have been possible. I would like to thank the coordinators of VIBOT Prof. Fabrice Meriaudeau, Prof. David Fofi, Prof. Yvan Petillot, and Prof. Robert Marti for their constant guidance. I would like to thank my supervisor Dr. Alain Lalande for his enormous support, guidance and patience for the success of this work. I would also like to thank the team of Medical Imaging laboratory and "Hôpital d' Enfants" for providing infrastructure, data and a friendly and conducive atmosphere for the research. I would like to specially thank my wife Mrs. Jhimli Mitra whose constant encouragement and support has made this work possible.

## REFERENCES

- [1] S. Allender, P. Scarborough, V. Peto, M. Rayner, J. Leal, R. L. Fernandez, and Alastair Gray, "European Cardio Vascular Disease Statistics 2008", 2008.
- [2] D. L. Pham, C. Xu, and J. L. Prince, "Current Methods in Medical Image Segmentation", *Annu. Rev. Biomed. Eng.*, vol. 2, 2000, pp. 315-337.
- [3] M. Kass, A. Witkin, and D. Terzopoulos, "Snakes:Active Contour Models", *International Journal of Computer Vision*, 1988, pp. 321-331.
- [4] D. Hearn and M. P. Baker, *Computer Graphics, C Version*, Second edition, Prentice Hall, 1996.
- [5] S. T. Acton and N. Ray, *Biomedical Image Analysis: Tracking*, First edition, Morgan and Claypool Publishers, USA, 2005.
- [6] L. Cohen and I. Cohen, "Finite element methods for active contour models and balloons for 2-D and 3-D images", *IEEE Trans. Pattern Anal. Machine Intell.*, vol. 15, no. 11, 1993, pp. 1131-1147.
- [7] L. Cohen, "On active contour models and balloons", *CVGIP Image Understand.*, vol. 52, no. 2, 1991, pp. 211-218.
- [8] C. Xu and J. L. Prince, "Snakes, Shapes, and Gradient Vector Flow", *IEEE Trans. on Image Processing*, vol. 7, no. 3, 1998, pp. 359-369.
- [9] R. C. Gonzalez and R. E. Woods, *Digital Image Processing*, Second edition, Pearson Education, Low Price Edition, 2002.
- [10] Y. Y. Wong, P. C. Yuen, and C. S. Tong, "Contour Length Terminating Criterion for Snake Model", *Pattern Recognition*, vol. 31, no. 5, 1998, pp. 597-606.